Particle-resolved instabilities in colloidal dispersions

Hartmut Löwen

For colloidal dispersions, recent progress in observing, understanding and describing instabilities resolved on the length scale of the individual particles is summarized. The instabilities are induced and triggered by external driving fields. Various kinds of instabilities are discussed, including the buckling transition of a colloidal monolayer, lane and band formation in oppositely driven binary mixtures, the classic Rayleigh–Taylor instability and clustering in rod-like systems under nonequilibrium. Particularly, the role of complementary approaches, like real-space experiments, computer simulations and theory is emphasized.

I. Introduction

Much of the complexity in nature occurs *via* instabilities from homogeneous states towards situations with much higher degrees of intrinsic ordering.[1] These hydrodynamic and thermodynamic instabilities[2] are conventionally described by coarse-grained continuum models, which consider the system on length scales much larger than a typical interparticle distance a. This is a satisfactory picture as long as the emerging structures are much larger than a, but it clearly breaks down for "microscopic" instability patterns formed on the interparticle distance scale. For the latter, full microscopic approaches are needed, which possess resolution on the corresponding microscopic length and time scales. The counterplay between the microscopic and macroscopic behaviour of instabilities is a topic of intense recent research, which will be addressed in this review.

Institut für Theoretische Physik II: Weiche Materie, Heinrich-Heine-Universität Düsseldorf, Universitätsstraße 1, D-40225, Düsseldorf, Germany

Hartmut Löwen

Hartmut Löwen studied physics at the University of Dortmund, Germany. In 1987, he received his PhD degree in physics from Dortmund University on phase transitions in polaron systems. He then moved to the Ludwig-Maximilians-Universität München where he worked on surface melting and classical density functional theory. During a postdoc stay in Lyon (France) he started to do research on colloidal dispersions. Since 1995 he is full professor for Theoretical Physics at the University of Düsseldorf (Germany). His research concerns theoretical descriptions and computer simulations of soft matter systems. He is coordinator of the German-Dutch collaborative research centre SFB-TR6 "Physics of Colloidal Dispersions in External Fields".

Soft matter represents a broad material class, which is vulnerable to small external perturbation and is thus susceptible to instabilities.[3] In particular, mesoscopic colloidal suspensions embedded in a molecular solvent are excellent model systems to observe instabilities on the particle scale, *i.e.* the emerging structure can be particle-resolved and watched in real-space.[4–11] This is intriguing for at least two reasons: first of all, new instabilities can occur on the particle scale, which possess no coarse-grained counterpart. One example is the buckling instability[12] of a confined crystalline layer,[13,14] which occurs, *per se*, on the interparticle scale. Buckling will be discussed in this review in section II. Secondly, it is intriguing to test the validity of a coarse-grained approach downwards to the "microscale" of interparticle distances.[15–17] Typically it is a challenging question to understand and characterize the conditions under which the phenomenology-based continuum approaches break down.

In this review, recent results about particle-resolved instabilities in colloidal dispersions are summarized. The instabilities discussed here are, in general, produced by external fields, such as electric, gravitational or topographical (confining) fields.[5,18] The external field couples directly to the individual colloidal particles and induces an external driving force on them which – together with their interparticle interaction force and Brownian dynamics – brings the suspensions into another state *via* an instability. This can occur both under equilibrium and nonequilibrium conditions. In equilibrium, instabilities manifest themselves typically *via* a continuous (second-order) phase transition. As a representative example for an equilibrium instability, the *buckling* transition of a confined colloidal monolayer will be discussed in this paper.[14] Further instabilities that occur at nonequilibrium are *laning* and *banding* in oppositely driven colloidal binary mixtures or the classical *Rayleigh–Taylor instability*,[2,19] where a colloidal suspension with a positive buoyant mass is placed above a pure solvent and is unstable due to gravity. Lastly, *clustering instabilities* can occur in driven and self-propelled suspensions of rod-like particles, which are genuine nonequilibrium situations. Under the action of external and internal fields, rod-like particles can aggregate into clusters and this can also be understood and classified as an instability. This review clearly cannot cover all aspects of colloidal instabilities. The following topics are not treated: kinetics of colloidal fluid-fluid phase separation,[20,21]

vorticity banding,[22,23] morphological instabilities of a growing interface near a solvent-freezing transition,[24] electro-convection effects,[25] the Rayleigh–Bernard instability[26] and all instabilities that concern the solvent flow, alone.

Scientific progress in understanding instabilities on the particle-scale has been achieved by using real-space experiments (typically confocal microscopy), see *e.g.* Refs 4, 6–8, 11 and 27–30, computer simulations[17,31,32] and theory.[33,34] Computer simulations need a proper inclusion of hydrodynamic interactions[35] mediated between the colloidal particles by solvent flow if the instabilities occur in nonequilibrium. Theories are either based on a linear stability analysis of phenomenology-based and hydrodynamical approaches or involve microscopic dynamical density functional approaches.[36–39] A direct comparison of the complementary approaches (experiment and simulation/theory) is possible, thereby facilitating a deepened understanding of the impact of individual particles on the instabilities.

The paper is organized as follows: First a simple instability in equilibrium, namely the buckling instability, is discussed in section 2. Then nonequilibrium instabilities follow in the subsequent sections III–VI including laning, banding, the Rayleigh–Taylor instability and clustering instabilities. Final conclusions are given in section VII.

II. The buckling instability

The *buckling* instability of a confined crystalline layer occurs if the circumstances of confinement are changed. In its simplest form, buckling shows up even at zero temperature and can therefore be understood in terms of purely potential energy arguments.[14,40] The situation of a buckling instability is sketched in Fig. 1 in two spatial dimensions where the solid layer is a one-dimensional periodic string of particles confined between two parallel lines. These strings can buckle into a zig-zag-like structure by either increasing the density or weakening the external confinement strength, *i.e.* it emerges from a competition of two energy scales, namely the confinement strength and the interparticle repulsion. At zero temperature, buckling can be studied with a perturbative approach assuming a small interlayer spacing h, which is a convenient order parameter for buckling. Typically, the buckling instability is a second-order phase transition, say at a critical density ρ_c. Close to ρ_c, the buckling order parameter h changes continuously as $h \simeq \sqrt{\rho - \rho_c}$ for $\rho > \rho_c$ while $h = 0$ for $\rho \leq \rho_c$.

The buckling instability can be detected on the particle scale for colloidal suspensions by real-space experiments.[41] Typically, these particles are confined between two parallel plates and the particles are observed by microscopy.[42–46] Alternatively, buckling has been identified by scattering methods.[47,48] Microscopy has the advantage that the lateral structure can be resolved directly. Scattering experiments[47,48] average over the lateral structure, but focus on the height variables of the particles in the slit perpendicular to the system walls.

The resulting buckling structure depends crucially on the wall-particle and the interparticle interaction. For the latter, both hard spheres and screened Coulomb (Yukawa) pair potentials have been considered. The former case is an appropriate model for sterically-stabilized colloidal suspensions. In the latter case, the interparticle pair potential $V(r)$ reads as
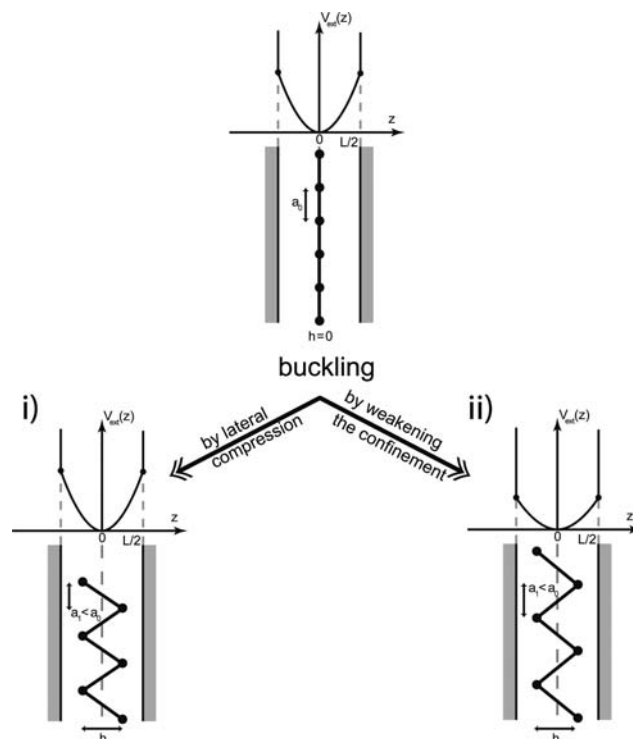
Fig. 1 A sketch of the buckling instability in two dimensions. Particles are confined by a strong confining potential $V_{ext}(z)$ in a linear channel forming a periodic string of a one-dimensional crystal with lattice constant a_0 at zero temperature. Layer buckling resulting in a zig-zag structure may occur (i) by compressing the layer laterally, which leads to an increased density per unit length (corresponding to a reduced interparticle spacing $a_1 < a_0$) and (ii) by weakening the confinement potential $V_{ext}(z)$ in the middle of the slit.

$$V(r) = \frac{V_0 \exp(-\kappa r)}{r} \quad (1)$$

where r is the interparticle spacing, κ is the inverse Debye–Hückel screening length and V_0 is an energy amplitude, which scales with the square of the particle effective charges. The Yukawa model is appropriate for charge-stabilized colloidal suspensions.[49–54] Besides hard-sphere and Yukawa interactions, other interactions, like Lennard-Jones and Gaussian potentials,[55–57] have also been considered for buckling. More crucial is the nature of the confining wall-particle external potential $V_{ext}(z)$. If this is hard, *i.e.*

$$V_{ext}(z) = \begin{cases} 0, & \text{for } -L/2 < z < L/2 \\ \infty, & \text{else} \end{cases} \quad (2)$$

with L denoting the plate distance, buckling occurs into a zig-zag structure of rows, which possesses a rectangular 2×1 cell.[58–62] This 1-1 bilayer structure shown in Fig. 2a) respects the inversion symmetry $z \rightarrow -z$ embodied in the external wall potential. The 1-1 bilayer buckling structure occurs for both hard sphere[58–60] and Yukawa interparticle potentials[63] and has been confirmed in various experiments on strongly confined colloidal suspensions, which are touching the confining walls.[41–45]

On the other hand, for a parabolic wall-particle external potential $V_{ext}(z)$
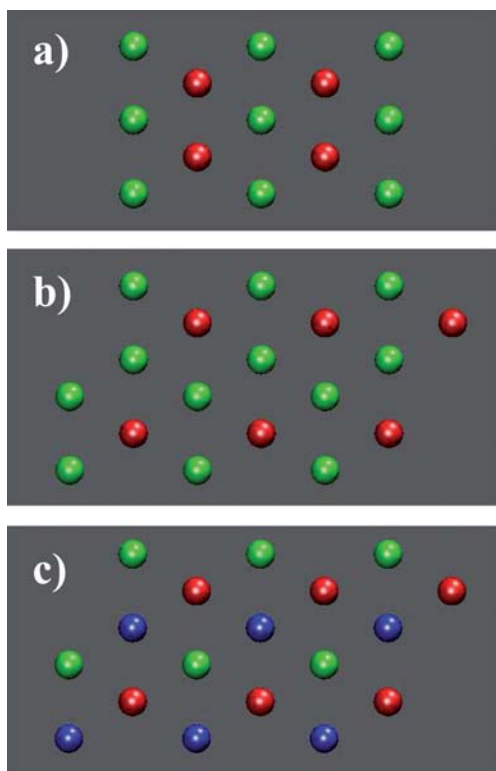
Fig. 2 Top views of the buckled structures starting from a triangular confined monolayer. (a) Symmetric 1-1 rows with a 2×1 structure, (b) a 2-1 structure with a $\sqrt{3} \times \sqrt{3}$ corrugation and (c) a 1-1-1 trilayer (3Δ). Particles in different layers are depicted with different colors.

$$V_{ext}(z) = \frac{1}{2} K_0 z^2 \qquad (3)$$

the situation is more subtle. The parabolic form is a reasonable model for charged colloids confined between strongly charged parallel walls at low salt concentrations.[51] Various lateral structures of the buckled layer have been suggested by Chou and Nelson[14] using a Landau-type theory for the total potential energy. One is an asymmetric 2-1 structure, which was confirmed in computer simulations.[55] This bilayer structure is characterized by a $\sqrt{3} \times \sqrt{3}$ corrugation, see Fig. 2b). It occurs genuinely if the interparticle potential is short-ranged. However, for long-ranged interparticle forces there is the possibility to buckle from a monolayer directly into a trilayer.[64] This 1-1-1 trilayer is symmetric (see Fig. 2c for a sketch of its structure). In principle, buckling could also occur into higher-order multilayers,[65] but this needs more elaboration. Interestingly, even the 2-1 structure still needs clear experimental confirmation.

Future research activities will focus on buckling of monolayers composed of two-component systems. For binary Yukawa systems, the ground-states of the monolayer have recently been identified for various screening strengths κ and charge asymmetries revealing a wealth of different lateral and compositional structures.[66] Correspondingly, one may expect much more complex lateral buckled structures.

Finally, the case of particles in strong gravity on a substrate is characterized by an external potential

$$V_{ext}(z) = \begin{cases} mgz, & \text{for } z > 0 \\ \infty, & \text{else} \end{cases} \qquad (4)$$

Here, the buckling transition of a crystalline monolayer is first-order with a jump in the height variables. This can clearly be seen for hard spheres where, for strong gravity, a layer-by-layer growth minimizes the potential energy if the areal density is increased. While the incomplete layers are highly degenerated for hard spheres, this is different for continuous interactions (like Yukawa systems). Here the scenario of buckling still needs to be explored in the future. Experiments[27] that realize "gravity" by using the light pressure acting on the colloidal particles have the advantage that the strength of gravity can easily be tuned and – when combined with confocal microscopy – are promising set-ups to detect the resulting buckled structures in real-space.

III. The laning instability

The *laning* instability (or two-stream instability) occurs if a binary mixture of particles are driven against each other. For the standard set-up, the driving force is constant

$$\vec{F} = \pm \vec{F}_0 \qquad (5)$$

but the sign is different for the different particle species. For strong enough driving forces $\vec{F}_0$, particles driven alike move behind each other in order to avoid collisions with oppositely driven particles. Correspondingly, long "chains" or "worms" of particles driven alike built up in the systems. Typical snapshots from a two-dimensional Brownian dynamics computer simulation[67] are shown in Fig. 3 both for low and high driving forces.

Colloidal suspensions are excellent model systems for the laning instability. Typically, the experiments are performed in a three-dimensional capillary cell. In fact, oppositely charged particles, driven in a constant electric field, exhibit lane formation,[69] for a confocal micrograph see Fig. 4. Therefore an electric field is an excellent realization for the drive in eqn (5).

In the following, recent progress to understand and characterize the laning instability is reviewed. First, Brownian dynamics computer simulations in two spatial dimensions for repulsive interparticle interactions have revealed that lane formation is a first-order phase transition,[67] *i.e.* it occurs with a notable
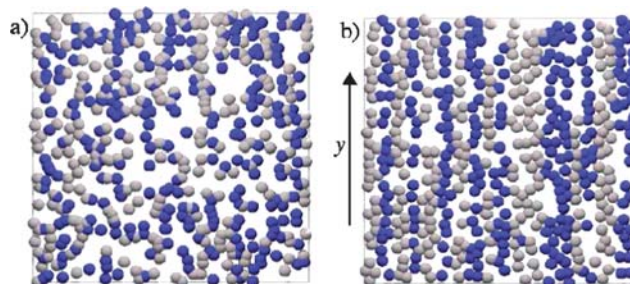

Fig. 3 Typical snapshots from a two-dimensional Brownian dynamics computer simulation for a binary driven Yukawa mixture at low and high driving forces $\vec{F}_0$. At high forces, the structure of lanes along the driving field can clearly be seen. The drive is along the *y*-direction. Without drive, both particle species are indistinguishable. Different colours represent particles that are driven alike. From ref. 68.
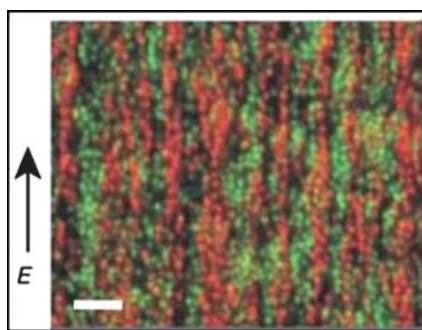
Fig. 4 A confocal micrograph of a three-dimensional, oppositely charged, colloidal mixture in an external electric field. The arrow shows the direction of the electric driving field. The particles are colored according to their charge. Lane formation along the drive can clearly be seen. The length bar is a micron. From ref. 69.

hysteresis if the field is increased and decreased. There is re-entry of the lane-free state for fixed drives and increasing density. For an example of the steady-state diagram, see Fig. 5. In fact, for increasing density and fixed driving strength, the sequence of steady states involves no lanes - lanes - no lanes.[68] The instability can be quantitatively described using dynamical density functional theory with an additional phenomenology-based current term.[70] However, a microscopic justification of this additional current term is still needed. Data obtained from a dynamical density functional theory are also included in Fig. 5.

More recent, extensive Brownian dynamics computer simulations[71] for oppositely charged hard-core Yukawa mixtures in three dimensions exhibit a much richer scenario of different steady states. For fixed driving strength, the steady-state diagram is summarized in Fig. 6. What is varied here is the colloid concentration as embodied in the total colloid packing fraction ϕ and the inverse Debye–Hückel screening length κ. Apart from a region in the parameter space where no laning occurs, namely for small density ϕ, there is a transition towards laning for any κ. A snapshot of particle positions projected on a plane perpendicular to the drive reveals the lateral order of the lanes. There is a network structure with a finite spacing at high κ.
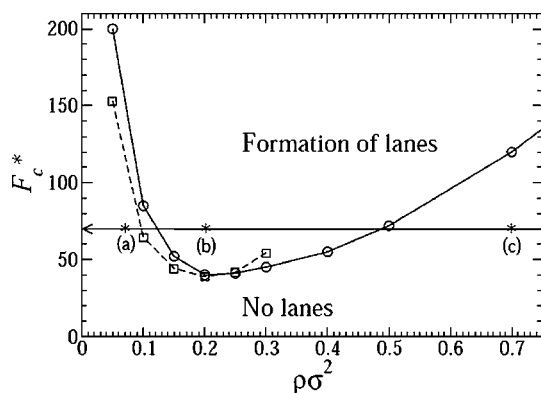
Fig. 5 A steady state diagram for laning in the parameter space of density (x-axis) and driving strength F_c^*. Computer simulation results (—) and data from dynamical density functional (---) are shown. The lines separate the parameter space into two regions: lane formation and no lane formation. (a), (b), and (c) denote three states along a path of constant force and increasing density. From ref. 68.
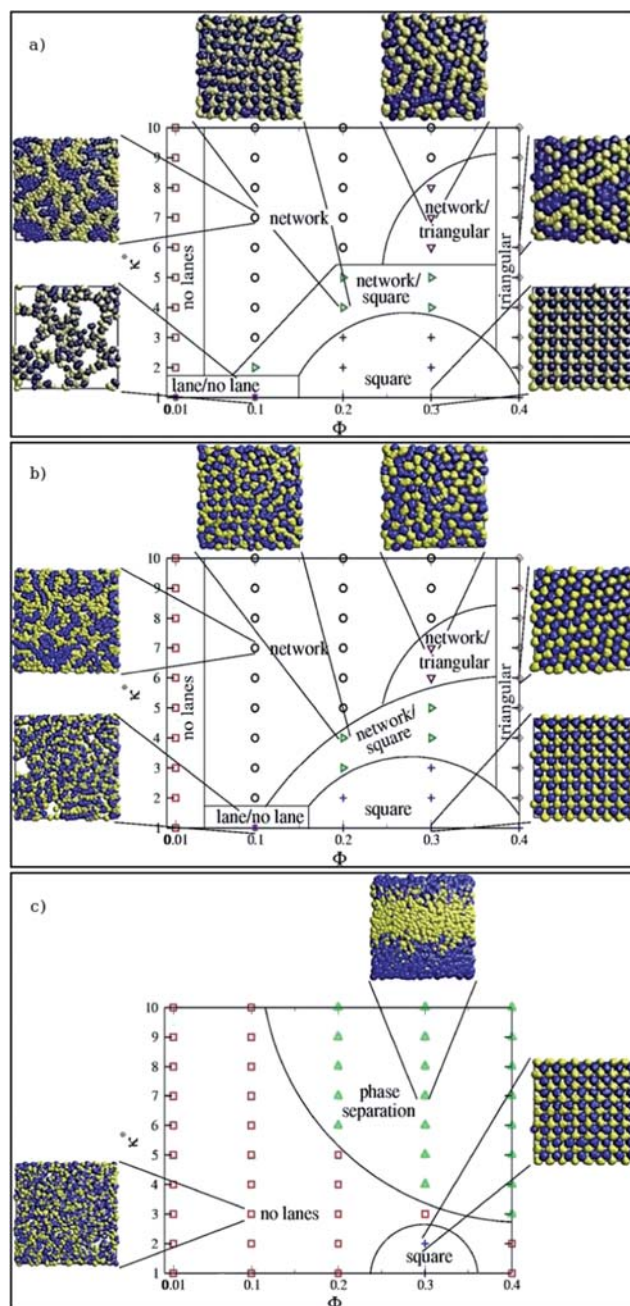
Fig. 6 A steady-state phase diagram of laning for an oppositely charged hard-core Yukawa interaction and fixed driving strength as a function of the particle volume fraction Φ and reduced screening parameter κ^* (a) for no hydrodynamic interactions, (b) for a driving electric field with the Long–Ajdari mobility tensor and (c) for a driving gravitational field with a Rotne–Prager mobility tensor. The snapshots represent projections on a plane perpendicular to the driving field and characterize the different steady-states. From ref. 72.

However, for lower κ, the lanes crystallize into two-dimensional lattices, which can possess triangular, rhombic and square structures. Finally, for small ϕ and small κ, chains of lanes are forming possibly on the way to complete phase separation towards a square crystal.

Since the moving colloidal particles induce a solvent velocity field, there is an issue about the importance of hydrodynamic

interactions mediated by the solvent flow. One can include them in their leading order by the long-ranged pairwise Rotne–Prager tensor[35] if the driving field is gravity or by the shorter-ranged Ajdari–Long tensor[73] if the driving field is electric. In the latter case, the long-ranged Oseen tensor is screened due to the counter-motion of counterions in the electric field, which is absent for a gravitational drive. Indeed, this guarantees[72] that hydrodynamic interactions do not destroy the topology of the steady-state diagram, shown in Fig. 6. However, for gravity (sedimentation), laning is connected with macroscopic phase separation and the stability range of a lateral lane crystal is strongly suppressed. The same qualitative difference occurs for the order of the laning instability. Simulation reveals that it is first order for sedimentation, but continuous (i.e. without any notable hysteresis) for a driving electric field.[74] The same is true for experiments on oppositely charged colloids in electric fields.

A further observation of lane formation has been recently found in dusty plasma clouds.[75] Small dust particles were injected with high speed into a cloud of big dust particles in experiments on the International Space Station.[76] In fact, for the given initial condition, both particles quickly form lanes and penetrate each other via laning, as demonstrated in Fig. 7. The degree of laning was characterized by an anisotropic scaling index and quantitative agreement was found with computer simulations. The simulations involve inertia and low friction for the particle dynamics and adopt a repulsive Yukawa form for their interactions.[76]

In conclusion, laning is an instability, which occurs on the particle scale, i.e. the size of the structures formed are of the order of interparticle distances. Therefore particle-resolved experiments, simulations and theories are needed to understand the details of laning. In the future, for laning in charged colloidal dispersions, a full simulational treatment of hydrodynamics and explicit microions is needed in order to elucidate the role of the electric dipole moments induced by the applied field. Modern simulation techniques,[77–81] which incorporate both hydrodynamics and electrostatics will be helpful in this respect.

IV. The banding instability

If particles segregate perpendicular to the driving field into bands, the associated instability is called *banding* (or axial segregation).[34,82] This has been recently observed both for periodically shaken granular matter[83–86] and in Brownian dynamics simulations, appropriate for colloidal suspensions in time-oscillatory external driving fields.[82] Here, the driving force is time-dependent and given by:

$$\vec{F}(t) = \pm \vec{F}_0 \cos(\omega t) \qquad (6)$$

where ω denotes the driving frequency and the two different signs correspond to two species of the particles, which are driven against each other. In the limit of $\omega \to 0$, one recovers a constant drive which, was discussed in the preceeding section, see eqn (5). The strength of the drive can be characterized by a dimensionless Peclet number Pe, which is defined as

$$Pe = F_0 \frac{\sigma}{2k_B T} \qquad (7)$$

where σ is the particle diameter and $k_B T$ the thermal energy.
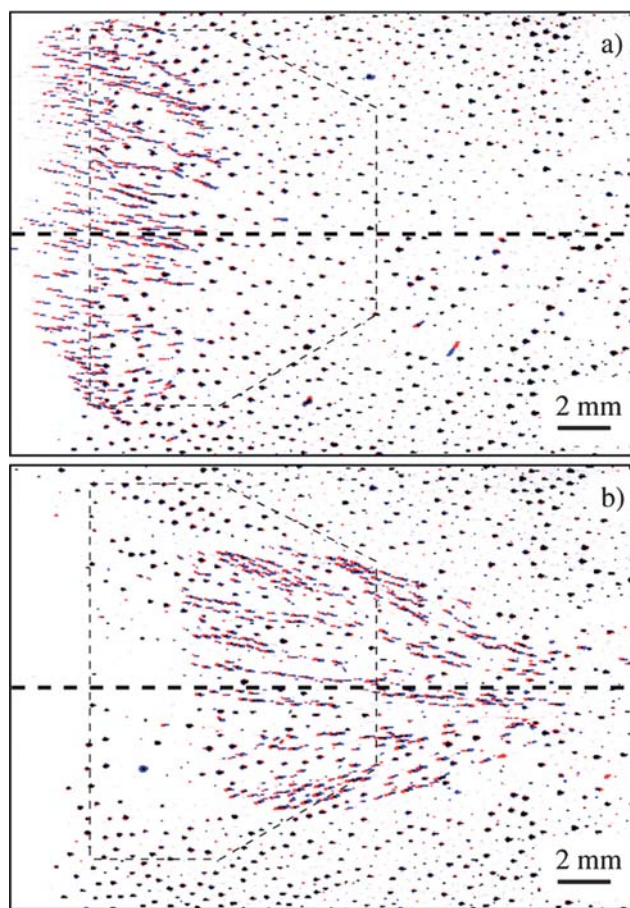
Fig. 7 Lane formation in complex plasmas. A short burst of small (3.4 μm) particles is injected into a cloud of big (9.2 μm) background particles (close to the midplane of the chamber, indicated by horizontal dashed line). Small particles are driven towards the center, stages of (a) initial lane formation and (b) merging of lanes into larger streams are shown. Particles are illuminated by a thin laser sheet of ≃0.35 mm; each figure is a superposition of two consecutive images (1/50 s apart), the time difference between them is ≃1.2 s. At stage (b), big particles also form well-defined lanes. The frame indicates the region used for the analysis of big-particle dynamics. From ref. 76.

An example for the emerging steady-state diagram in a plane spanned by the driving frequency ω and the Peclet number Pe is shown in Fig. 8. Banding occurs for intermediate parameters and is followed by laning for higher Peclet numbers. On the other hand, there is no pattern formation for small Peclet numbers and high frequencies. This becomes immediately clear by observing that high frequencies lead to an almost vanishing net force if the time-scale of the external drive is much faster than the viscous response time of the particles. The intuitive mechanism for banding is that particles driven alike perform the same harmonic excursions induced by the external field. It is more profitable for the system to arrange into bands since there are only two big collision events involving two oppositely driven bands during one oscillation cycle, which is preferred to a steady friction of lanes. Since banding is a highly collective process, the formation of bands needs a long time, i.e. many oscillation cycles if started from a completely mixed configuration. Finally, the tilted bands
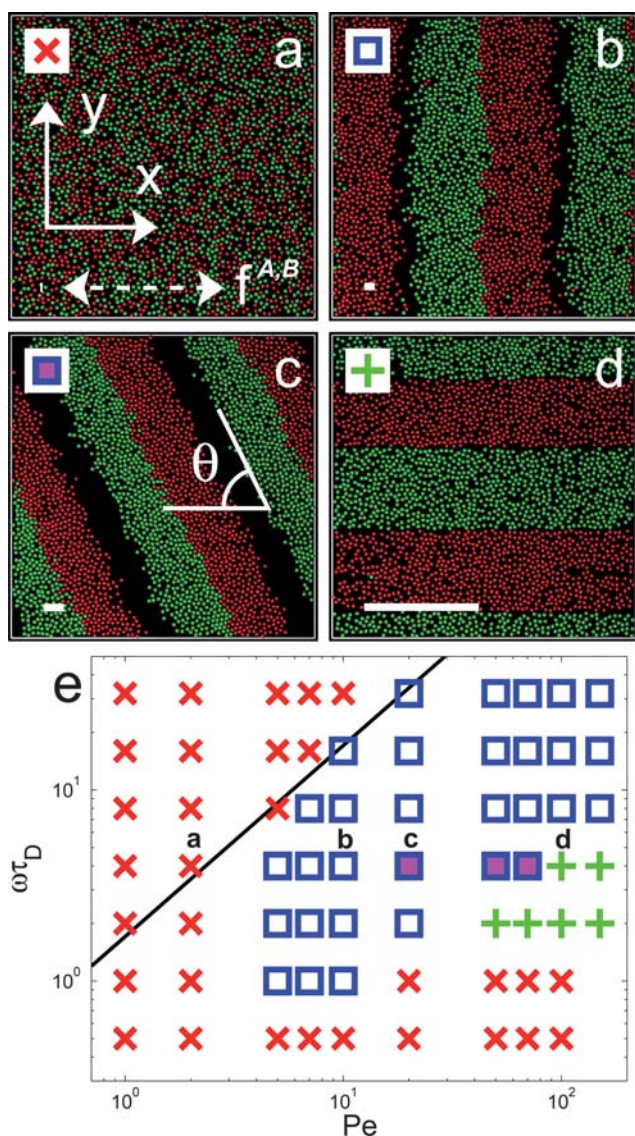
Fig. 8 [(a)–(d)] BD simulation snapshots for fixed driving frequency $\omega\tau_D = 4$ (τ_D denoting a typical diffusive time scale) but different Peclet numbers Pe after 10^4 periods starting from a fully mixed configuration. Particles colored in green are of species A while particles colored in red are of species B. Symbols in the left upper corner correspond to symbols used in (e). In (a) the coordinate frame is shown and the direction of the driving field is indicated by the broken arrow. In [(a)–(d)] the length of the solid bars (bottom left corner) correspond to the amplitude of a free particle driven without noise in the external field. For small Pe, a disordered state (a) is observed, for intermediate Pe, colloids segregate into stripes oriented perpendicular or tilted (tilt angle θ) to the direction of the oscillating force [(b)–(c)], on the other hand, for high Pe, lanes are formed parallel to the direction of the oscillatory force (d). Parameters are $\omega\tau_D = 4$ and $Pe = 2, 10, 20, 110$ from (a) to (d). (e) A nonequilibrium steady-state phase diagram for fixed area fraction $\phi = 0.4$. The solid line describes a simple theoretical estimate of the disordered-to-segregated phase boundary. The parameters of the snapshots [(a)–(d)] are also indicated, and $f^{A, B} = \pm F_0$. From ref. 82.

seen in the simulations might be artifacts of the periodic boundary conditions used in the simulations.

A theoretical description, as well as an experimental realization, of banding in the colloidal context is a challenging task for the future. Since banding appears as a secondary instability on top of initial laning, a theoretical description is not easy and probably needs terms beyond a linear stability analysis.[33]

V. The Rayleigh–Taylor instability

If a heavy liquid is placed above a lighter one, it is unstable since the system will tend to minimize its potential energy. The classical *Rayleigh–Taylor instability* is a fingering instability and results from a growth of unstable interface fluctuations. In fact, typically, there are two competing mechanisms that determine the stability of the interface: surface tension due to an increase of the interfacial area, which will work against a growing interface, and potential energy, which tends to destabilize the sample. For the simple, two-dimensional situation shown in Fig. 9, where a periodic undulation of the interface with an amplitude h_0 and wavelength λ is shown, the increase in line tension γ per unit length is proportional to $\pi^2 h_0^2 \gamma/\lambda^2$, while the potential energy gain per unit length is λ-independent and given by $h_0^2 g(m_1\rho_1 - m_2\rho_2)$ where $(m_1\rho_1 - m_2\rho_2) > 0$ measures the mass density contrast between the upper and lower liquid and g denotes the gravitational acceleration. Therefore, there is a critical wavelength

$$\lambda_c = \sqrt{\frac{\pi^2\gamma}{g(m_1\rho_1 - m_2\rho_2)}} \qquad (8)$$

which separates a stable from an unstable regime: interface undulations with $\lambda > \lambda_c$ are unstable while for $\lambda < \lambda_c$ they are stable. Clearly, if the surface (or line) tension is zero, **all** undulations are unstable.

In the initial (linear) regime, unstable modes grow exponentially in time $\propto \exp(n(\lambda)t)$. The actual growth rates $n(\lambda)$ can be obtained from a study of the Navier–Stokes equations[2] revealing a maximal unstable one, *i.e.* the growth rate $n(\lambda)$ exhibits a maximum at a finite wavelength λ_m. The latter mode will clearly dominate after finite time such that the interfacial structure should exhibit a peak in its Fourier transform close to $2\pi/\lambda_m$.

The physical reason for the maximal growth rate is obvious and explained as follows. Consider the case of vanishing surface tension, $\gamma = 0$ first. As $\lambda \to 0$ much mass diffusion is needed to grow the undulation, hence $n(\lambda \to 0) = 0$. On the other hand, for $\lambda \to \infty$, viscous friction of the opposite layers will slow down the motion, implying $n(\lambda \to \infty) = 0$. Therefore, in between, there must be a maximal growth rate.

It is an intriguing question, how the classical Rayleigh–Taylor instability looks on the particle scale where continuum concepts
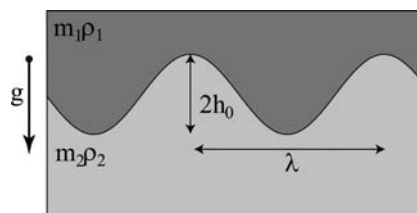
Fig. 9 A sketch of the classical Rayleigh–Taylor instability. A heavy liquid (dark grey) is placed above a lighter liquid (light grey), $m_1\rho_1 > m_2\rho_2$, and an interface fluctuation with a wavelength λ is considered. For $\lambda > \lambda_c$, the situation is unstable.

like surface tension γ and viscosity *etc.* break down. Here colloidal dispersions mark the dividing line between molecular systems who typically do not feel gravity on single particles and granulates for which a typical thermal energy is neglected against gravity. The actual impact of gravity can again be characterized by the Peclet number

$$Pe = \frac{mg\sigma}{k_BT} \tag{9}$$

where σ is the particle diameter. For granular systems,[87,88] $Pe \gg 1$, while for colloids Pe is of the order of unity.

Recent investigations of the Rayleigh–Taylor instability were performed for sterically-stabilized spherical colloidal suspensions, which can be modelled as hard spheres.[17,89–91] Under gravity, the suspension sediments to the bottom of the sample leaving a couple of layers there. When the sample is quickly turned upside down, the set-up for a Rayleigh–Taylor instability is realized. However, there is no surface tension γ in this case, which leads to the expectation that all undulations are unstable. Experimental data within an observation slice containing the gravity direction $\vec{g}$ and perpendicular to it are presented in Fig. 10.

The sedimentation experiments were performed in a slit-like geometry. The slit width L was about 20–30 times the hard sphere diameter. While qualitative agreement is achieved between the experimental data and computer simulations, which include hydrodynamic interactions between the colloids by using the multiparticle-collision dynamics,[32,92] quantitative agreement
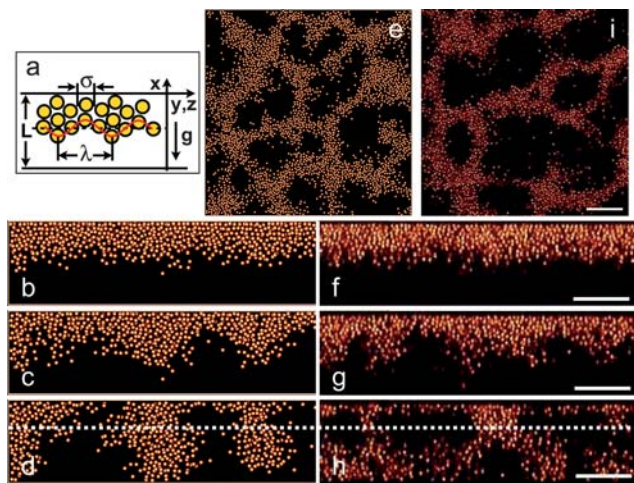
Fig. 10 (a) A schematic illustrating the spatial parameters σ, λ and L. (b–e) Simulation snapshots of a system, which contains $N = 433858$ colloidal particles in a simulation box with dimensions $L/\sigma = 18$ and $L_y/\sigma = L_z/\sigma = 81$. The value of the Peclet number is $Pe = 1.6$. (b–d) The time series of the system at time $t/\tau_S = 3.2(b)$, $6.4(c)$, $9.6(d)$. τ_S is the time a single particle needs to sediment over its own radius. The snapshots are slices of thickness 2σ done in the xy plane. (e) A slice of thickness 2σ in the yz plane at time $t/\tau_S = 9.6$. The height of the yz plane is $x/L = 2/3$, as indicated by the dashed line in (d). (f–i) The experimental realisation of the Rayleigh–Taylor-like instability. (f–h) A time series of images taken with a confocal microscope in the xy plane for the volume fraction $\phi = 0.15$, and $Pe = 1.1$ and $L/\sigma = 18$ at times $t/\tau_S = 1.43(f)$, $5.5(g)$, $11.22(h)$. (i) A slice in the yz plane at a height $x/L = 2/3$ (indicated by the dashed line in (h)) at time $t/\tau_S = 11.22$. In (f–i) the scale bars denote 40 μm. (f–h) are 2D images reconstructed from 3D confocal scans. From ref. 17.

can be seen in the wavenumber-resolved initial growth rates of interfacial fluctuations. An example is shown in Fig. 11. Experimental data (filled symbols) agree with computer simulations (open symbols). The solid lines are the predictions of a linearized stability theory based on the Navier–Stokes equation.[2,17] It can be concluded that a colloid diffusion correction $\propto -Dk^2$ is needed to get agreement between the experimental and simulational growth rates, Here, D denotes the colloid diffusion coefficient and $k = 2\pi/\lambda$ the wavenumber. Nevertheless, there is amazing agreement between theory and experimental/simulation, showing that the coarse-grained Navier–Stokes equations are valid almost down to "microscopic" (*i.e.* interparticle) length scales.

Alternate observations of the Rayleigh–Taylor instability on the particle scale are experiments of colloids in a dielectric bottle[93] and for colloid-polymer mixtures with finite surface tension.[94] But here, a quantitative comparison to simulation and theory has not yet performed.

Finally a connection between the Rayleigh–Taylor instability and the laning instability was pointed out in ref. 19. In contrast to molecular dynamics,[95] for colloidal particles, which are described by Brownian dynamics, the laning instability is the ultimate limit of the Rayleigh–Taylor instability if the fastest growing undulation wavelength is comparable to the interparticle distance. In this sense, lane formation can be viewed as the particle-resolved Rayleigh–Taylor instability. The result in ref. 19 was gained for a two-dimensional model for colloids under the absence of hydrodynamic interactions. In three spatial dimensions, the relation between the Rayleigh–Taylor and the laning instabilities still needs to be explored.

VI. Clustering instabilities in rod-like suspensions under nonequilibrium

Rod-like particles offer more possibilities for equilibrium phases than spherical ones. Their phase diagram typically includes liquid-crystalline phases which possess translational and orientational order at various degrees. Correspondingly, in nonequilibrium, if rods are driven by external forces, there are even richer scenarios for instabilities, which can manifest themselves by mutual rod alignment and by accompanied cluster formation. In
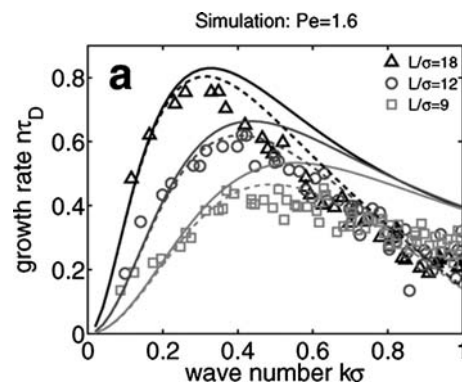
Fig. 11 The growth rate $n\tau_D$ versus wave number $k\sigma = 2\pi\sigma/\lambda$. Simulation results of $n(k)$ for different wall separation distances $L/\sigma = 18$, 12, 9 and fixed $Pe = 1.6$. τ_D is the time a single particle needs to diffuse over its own radius. From ref. 17.

particular, in two spatial dimensions, the mutual alignment effect is strongly pronounced if rods are approaching each other. In this context, Brownian dynamics computer simulations have been useful to explore and discover cluster formation in driven rod-like colloids in two dimensions. We shall focus on two examples in the following.

First, if a spherical particle is slowly driven through a two-dimensional nematic phase[96] perpendicular to the nematic director, it will locally destroy the nematic order and leave a trail behind it, which will again relax back to equilibrium nemtic order. In ref. 97, it was shown that this situation, however, is unstable at higher drives and exhibits a *clustering instability*: beyond a critical drive, rods will accumulate *in front of* the particle. Once a rod is pushed by the particle, it will need some time to rotate around the particle. During this time, more rods will be swept up by the particle such that a cluster is quickly forming. If the growing cluster exceeds a certain size, it rotates as a whole around the driven particle and the process starts again. Therefore the cluster formation is rhythmic in time, *i.e.* a typical frequency can be identified, which is associated with the cluster formation and release. The rhythmic clustering scenario was also obtained within a simple phenomenology-based theory in quantitative agreement with the computer simulations.[97] Though the clustering instability is quite general, it has not yet been confirmed in experiments on nematic films.[98]

Second, a clustering instability was found in self-propelled particles[99–101] upon confinement in microchannels. Rods were studied, which move along their orientational axis and perform Brownian motion.[102] Once such a self-propelled rod is hitting the wall, it needs some time to align to the wall. If other particles are approaching, they will get stopped and then self-assemble into a rod cluster, which has a hedgehog-like shape. Clearly this *hedgehog clustering instability* is an out-of-equilibrium phenomenon. It was confirmed by dynamical density functional theory[102] and should show up in various confining geometries.

In general, one may expect cluster formation in driven rod-like particle suspensions for very general circumstances if some kind of confinement is involved[103] and the drive is strong. A prominent recent example concerns self-starting micromotors of objects, which have the shape of a "cogwheel" in a bath of self-propelling particles.[104] The unusual collective effects of active rods can be exploited for sorting and filtering devices in mixtures.[105,106]

VII.   Conclusions

In conclusion, colloidal dispersions are ideal model systems to see instabilities on the particle scale. The individual colloidal positions can be resolved and watched in real-space. Consequently, "microscopic" information is available in order to understand various instabilities. This is, by now, well-established for thermodynamic instabilities, such as phase separation by spinodal decomposition[107–109] as well as crystallization and glass formation,[110,111] as obtained on the particle-level in pure colloidal dispersion or in colloid/polymer mixtures. In this review, the same idea was put forward for instabilities that are generated by employing external driving fields. Examples of these instabilities included buckling, laning, banding, fingering and "active" clustering.
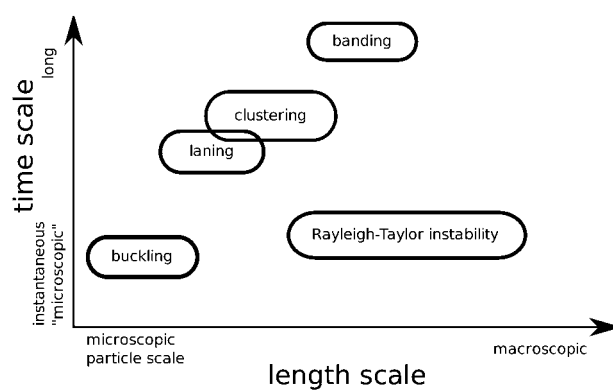
Fig. 12 A schematic overview of the instabilities discussed in this paper in terms of length scales on which the pattern exhibits a structure and of time scales on which these structures form for an unperturbed starting configuration.

Fig. 12 summarizes the key length and time scale upon which the instabilities are formed if an unperturbed situation is chosen as an initial configuration. While the undulation length of the Rayleigh–Taylor instability spans to macroscopic length scales depending on the actual system parameters, all other instabilities occur on the particle scale. As far as time scales are concerned, the banding instability took most time in order to develop completely while buckling is almost instantaneous.

There are many more examples that are beyond the scope of this review. To mention just a few, there is shear-banding for sheared suspensions[112] (*i.e.* a banding into coexistence regions with different internal shear rates). Related to buckling is the Asaro–Tiller–Grinfeld[113,114] instability of a strained solid film, which was recently explored by calculations on the particle scale.[115,116] Furthermore, other hydrodynamic instabilities, like the Marangoni effect,[117,118] can be seen directly on the particle scale for colloids. Temperature fields can be imposed to induce instabilities based on thermophoresis.[118–120]

Apart from the buckling instability, the situations discussed here involve fluid (disordered) phases. One could imagine much more complicated scenarios where solids are involved. Laning and banding can be studied for solid systems[121] with novel reentrant phenomena emerging, in particular if several crystalline phases are competing.[122] Colloidal dispersions will provide excellent model systems to explore these questions in the future.

Acknowledgements

References

1 M. C. Cross and P. C. Hohenberg, *Rev. Mod. Phys.*, 1993, **65**, 851.
2 S. Chandrasekhar, *Hydrodynamic and Hydromagnetic Stability*, Oxford University Press, Oxford, 1961.
3 E. Dickinson, *Soft Matter*, 2006, **2**, 642–652.

4 U. Gasser, E. R. Weeks, A. Schofield, P. N. Pusey and D. A. Weitz, *Science*, 2001, **292**, 258–262.

5 H. Löwen, *J. Phys.: Condens. Matter*, 2001, **13**, R415.

6 V. W. A. de Villeneuve, R. P. A. Dullens, D. G. A. L. Aarts, E. Groeneveld, J. H. Scherff, W. K. Kegel and H. N. W. Lekkerkerker, *Science*, 2005, **309**, 1231.

7 M. Klokkenburg, R. P. A. Dullens, W. K. Kegel, B. H. Erne and A. P. Philipse, *Phys. Rev. Lett.*, 2006, **96**, 037203.

8 R. P. A. Dullens, *Soft Matter*, 2006, **2**, 805.

9 A. Yethiraj, *Soft Matter*, 2007, **3**, 1099.

10 M. C. Jenkins and S. U. Egelhaaf, *Adv. Colloid Interface Sci.*, 2008, **136**, 65.

11 C. P. Royall, E. C. M. Vermolen, A. van Blaaderen and H. Tanaka, *J. Phys.: Condens. Matter*, 2008, **20**, 404225.

12 J. Genzer and J. Groenewold, *Soft Matter*, 2006, **2**, 310.

13 M. Delaye, R. Ribotta and G. Durand, *Phys. Lett. A*, 1973, **44**, 139.

14 T. Chou and D. R. Nelson, *Phys. Rev. E: Stat. Phys., Plasmas, Fluids, Relat. Interdisc. Top.*, 1993, **48**, 4611.

15 D. G. A. L. Aarts, M. Schmidt and H. N. W. Lekkerkerker, *Science*, 2004, **304**, 847.

16 C. P. Royall, J. Dzubiella, M. Schmidt and A. van Blaaderen, *Phys. Rev. Lett.*, 2007, **98**, 188304.

17 A. Wysocki, C. P. Royall, R. Winkler, G. Gompper, H. Tanaka, A. van Blaaderen and H. Löwen, *Soft Matter*, 2009, **5**, 1340.

18 H. Löwen, *J. Phys.: Condens. Matter*, 2008, **20**, 404201.

19 A. Wysocki and H. Löwen, *J. Phys.: Condens. Matter*, 2004, **16**, 7209.

20 B. Lu and A. R. Denton, *Phys. Rev. E: Stat., Nonlinear, Soft Matter Phys.*, 2007, **75**, 061403.

21 B. Zoetekouw and R. van Roij, *Phys. Rev. Lett.*, 2006, **97**, 258302.

22 K. Kang, M. P. Lettinga and J. K. G. Dhont, *Rheol. Acta*, 2008, **47**, 499–508.

23 J. K. G. Dhont and W. J. Briels, *Rheol. Acta*, 2008, **47**, 257–281.

24 S. S. L. Peppin, J. A. W. Elliott and M. G. Worster, *J. Fluid Mech.*, 2006, **554**, 147–166.

25 Y. L. Han and D. G. Grier, *J. Chem. Phys.*, 2006, **125**, 144707.

26 D. Velegol, S. Shori and C. E. Snyder, *Ind. Eng. Chem. Res.*, 2009, **48**, 2414–2421.

27 M. C. Jenkins and S. U. Egelhaaf, *J. Phys.: Condens. Matter*, 2008, **20**, 404220.

28 C. P. Royall, A. A. Louis and H. Tanaka, *J. Chem. Phys.*, 2007, **127**, 044507.

29 Y. L. Wu, D. Derks, A. van Blaaderen and A. Imhof, *Proc. Natl. Acad.Sci. U. S. A.*, 2009, **106**, 10564–10569.

30 D. Derks, Y. L. Wu, A. van Blaaderen and A. Imhof, *Soft Matter*, 2009, **5**, 1060–1065.

31 A. J. C. Ladd, *Phys. Rev. Lett.*, 1993, **70**, 1339.

32 A. Malevanets and R. Kapral, *J. Chem. Phys.*, 1999, **110**, 8605.

33 B. Schmittmann and R. K. P. Zia, *Statistical mechanics of driven diffusive system*, vol. 17, Academic Press, London, 1995.

34 I. S. Aranson and L. S. Tsimring, *Rev. Mod. Phys.*, 2006, **78**, 641.

35 J. K. G. Dhont, *An Introduction to Dynamics of Colloids*, Elsevier, Amsterdam, 1996.

36 U. M. B. Marconi and P. Tarazona, *J. Chem. Phys.*, 1999, **110**, 8032.

37 A. J. Archer and R. Evans, *J. Chem. Phys.*, 2004, **121**, 4246.

38 M. Rex and H. Löwen, *Phys. Rev. Lett.*, 2008, **101**, 148302.

39 M. Rex and H. Löwen, *Eur. Phys. J. E*, 2009, **28**, 139.

40 M. Medina-Noyala and B. I. Ivlev, *Phys. Rev. E: Stat. Phys., Plasmas, Fluids, Relat. Interdisc. Top.*, 1995, **52**, 6281–6288.

41 C. A. Murray and D. G. Grier, *Annu. Rev. Phys. Chem.*, 1996, **47**, 421–462.

42 J. A. Weiss, D. W. Oxtoby, D. G. Grier and C. A. Murray, *J. Chem. Phys.*, 1995, **103**, 1180–1190.

43 S. Neser, C. Bechinger, P. Leiderer and T. Palberg, *Phys. Rev. Lett.*, 1997, **79**, 2348–2351.

44 A. B. Fontecha, H. J. Schöpe, H. König, T. Palberg, R. Messina and H. Löwen, *J. Phys.: Condens. Matter*, 2005, **17**, S2779.

45 A. B. Fontecha, T. Palberg and H. J. Schöpe, *Phys. Rev. E: Stat., Nonlinear, Soft Matter Phys.*, 2007, **76**, 050402.

46 H. Löwen, A. Härtel, A. B. Fontecha, H. J. Schöpe, E. Allahyarov and T. Palberg, *J. Phys.: Condens. Matter*, 2008, **20**, 404221.

47 K. Nygård, D. K. Satapathy, J. Buitenhuis, E. Perret, O. Bunk, C. David and J. F. van der Veen, *Europhys. Lett.*, 2009, **86**, 66001.

48 D. K. Satapathy, K. Nygård, O. Bunk, K. Jefimovs, E. Perret, A. Diaz, F. Pfeiffer, C. David and J. F. van der Veen, *Europhys. Lett.*, 2009, **87**, 34001.

49 E. Allahyarov, H. Löwen and S. Trigger, *Phys. Rev. E: Stat. Phys., Plasmas, Fluids, Relat. Interdisc. Top.*, 1998, **57**, 5818–5824.

50 H. Löwen and E. Allahyarov, *J. Phys.: Condens. Matter*, 1998, **10**, 4147.

51 E. Allahyarov, I. D'Amico and H. Löwen, *Phys. Rev. E: Stat. Phys., Plasmas, Fluids, Relat. Interdisc. Top.*, 1999, **60**, 3199.

52 J.-P. Hansen and H. Löwen, *Annu. Rev. Phys. Chem.*, 2000, **51**, 209.

53 R. Messina, *J. Phys.: Condens. Matter*, 2009, **21**, 113102.

54 F. Bitzer, T. Palberg, H. Löwen, R. Simon and P. Leiderer, *Phys. Rev. E: Stat. Phys., Plasmas, Fluids, Relat. Interdisc. Top.*, 1994, **50**, 2821.

55 H. Bock, K. E. Gubbins and K. G. Ayappa, *J. Chem. Phys.*, 2005, **122**, 094709.

56 T. Das, S. Sengupta and S. Sinha, *J. Phys.: Condens. Matter*, 2009, **21**, 195408.

57 M. Kahn, J.-J. Weis, C. N. Likos and G. Kahl, *Soft Matter*, 2009, **5**, 2852–2857.

58 M. Schmidt and H. Löwen, *Phys. Rev. Lett.*, 1996, **76**, 4552.

59 M. Schmidt and H. Löwen, *Phys. Rev. E: Stat. Phys., Plasmas, Fluids, Relat. Interdisc. Top.*, 1997, **55**, 7228.

60 A. Fortini and M. Dijkstra, *J. Phys.: Condens. Matter*, 2006, **18**, L371.

61 Y. L. Han, Y. Shokef, A. M. Alsayed, P. Yunker, T. C. Lubensky and A. G. Yodh, *Nature*, 2008, **456**, 898–903.

62 Y. Shokef and T. C. Lubensky, *Phys. Rev. Lett.*, 2009, **102**, 048303.

63 R. Messina and H. Löwen, *Phys. Rev. Lett.*, 2003, **91**, 146101.

64 E. C. Oğuz, R. Messina and H. Löwen, *J. Phys.: Condens. Matter*, 2009, **21**, 424110.

65 E. C. Oğuz, R. Messina and H. Löwen, *Europhys. Lett.*, 2009, **86**, 28002.

66 L. Assoud, R. Messina and H. Löwen, *J. Chem. Phys.*, 2008, **129**, 164511.

67 J. Dzubiella, G. P. Hoffmann and H. Löwen, *Phys. Rev. E: Stat., Nonlinear, Soft Matter Phys.*, 2002, **65**, 021402.

68 J. Chakrabarti, J. Dzubiella and H. Löwen, *Phys. Rev. E: Stat., Nonlinear, Soft Matter Phys.*, 2004, **70**, 012401.

69 M. E. Leunissen, C. G. Christova, A. P. Hynninen, C. P. Royall, A. I. Campbell, A. Imhof, M. Dijkstra, R. van Roij and A. van Blaaderen, *Nature*, 2005, **437**, 235.

70 J. Chakrabarti, J. Dzubiella and H. Löwen, *Europhys. Lett.*, 2003, **61**, 415.

71 M. Rex and H. Löwen, *Phys. Rev. E: Stat., Nonlinear, Soft Matter Phys.*, 2007, **75**, 051402.

72 M. Rex and H. Löwen, *Eur. Phys. J. E*, 2008, **26**, 143–150.

73 D. Long and A. Ajdari, *Eur. Phys. J. E*, 2001, **4**, 29.

74 M. Rex, C. P. Royall, A. van Blaaderen and H. Löwen, 2008, http://arxiv.org/abs/0812.0908.

75 A. V. Ivlev, S. K. Zhdanov, H. M. Thomas and G. E. Morfill, *Europhys. Lett.*, 2009, **85**, 45001.

76 K. R. Sütterlin, A. Wysocki, A. V. Ivlev, C. Räth, H. M. Thomas, M. Rubin-Zuzic, W. J. Goedheer, V. E. Fortov, A. M. Lipaev, V. I. Molotkov, O. F. Petrov, G. E. Morfill and H. Löwen, *Phys. Rev. Lett.*, 2009, **102**, 085003.

77 J. Horbach and D. Frenkel, *Phys. Rev. E: Stat., Nonlinear, Soft Matter Phys.*, 2001, **64**, 061507.

78 H. Kodama, K. Takeshita, T. Araki and H. Tanaka, *J. Phys.: Condens. Matter*, 2004, **16**, L115.

79 V. Lobaskin, B. Dünweg and C. Holm, *J. Phys.: Condens. Matter*, 2004, **16**, S4063.

80 V. Lobaskin, B. Dünweg, M. Medebach, T. Palberg and C. Holm, *Phys. Rev. Lett.*, 2007, **98**, 176105.

81 Y. Nakayama, K. Kim and R. Yamamoto, *Eur. Phys. J. E*, 2008, **26**, 361.

82 A. Wysocki and H. Löwen, *Phys. Rev. E: Stat., Nonlinear, Soft Matter Phys.*, 2009, **79**, 041408.

83 T. Mullin, *Phys. Rev. Lett.*, 2000, **84**, 4741.

84 P. Sánchez, M. R. Swift and P. J. King, *Phys. Rev. Lett.*, 2004, **93**, 184302.

85 M. P. Ciamarra, A. Coniglio and M. Nicodemi, *Phys. Rev. Lett.*, 2005, **94**, 188001.

86 M. P. Ciamarra, A. Coniglio and M. Nicodemi, *Eur. Phys. J. E*, 2007, **22**, 227.

87 C. Völtz, W. Pesch and I. Rehberg, *Phys. Rev. E: Stat., Nonlinear, Soft Matter Phys.*, 2001, **65**, 011404.
88 J. L. Vinningland, O. Johnsen, E. G. Flekkøy, R. Toussaint and K. J. Måløy, *Phys. Rev. Lett.*, 2007, **99**, 048001.
89 C. P. Royall, J. Dzubiella, M. Schmidt and A. van Blaaderen, *Phys. Rev. Lett.*, 2007, **98**, 188304.
90 M. Schmidt, C. P. Royall, A. van Blaaderen and J. Dzubiella, *J. Phys.: Condens. Matter*, 2008, **20**, 494222.
91 A. Wysocki, C. P. Royall, R. Winkler, G. Gompper, H. Tanaka, A. van Blaaderen and H. Löwen, *Faraday Discuss.*, 2010, **144**, 245–252.
92 J. T. Padding and A. A. Louis, *Phys. Rev. E: Stat., Nonlinear, Soft Matter Phys.*, 2008, **77**, 011402.
93 J. Zhao, D. Vollmer, H.-J. Butt and G. K. Auernhammer, *J. Phys.: Condens. Matter*, 2008, **20**, 404212.
94 D. G. A. L. Aarts, R. P. A. Dullens and H. N. W. Lekkerkerker, *New J. Phys.*, 2005, **7**, 40.
95 J. L. Barber, K. Kadau, T. C. Germann and B. J. Alder, *Eur. Phys. J. B*, 2008, **64**, 271–276.
96 R. L. C. Vink, *Phys. Rev. Lett.*, 2007, **98**, 217801.
97 H. H. Wensink and H. Löwen, *Phys. Rev. Lett.*, 2006, **97**, 038303.
98 U. Delabre, C. Richard and A. M. Cazabat, *J. Phys. Chem. B*, 2009, **113**, 3647.
99 J. Toner, Y. H. Tu and S. Ramaswamy, *Ann. Phys.*, 2005, **318**, 170.
100 P. Hänggi and F. Marchesoni, *Rev. Mod. Phys.*, 2009, **81**, 387.
101 A. Erbe, M. Zientara, L. Baraban, C. Kreidler and P. Leiderer, *J. Phys.: Condens. Matter*, 2008, **20**, 404215.
102 H. H. Wensink and H. Löwen, *Phys. Rev. E: Stat., Nonlinear, Soft Matter Phys.*, 2008, **78**, 031409.
103 S. van Teeffelen and H. Löwen, *Phys. Rev. E: Stat., Nonlinear, Soft Matter Phys.*, 2008, **78**, 020101.
104 L. Angelani, R. D. Leonardo and G. Ruocco, *Phys. Rev. Lett.*, 2009, **102**, 048104.
105 M. B. Wan, C. J. O. Reichhardt, Z. Nussinov and C. Reichhardt, *Phys. Rev. Lett.*, 2008, **101**, 018102.
106 S. E. Hulme, W. R. DiLuzio, S. S. Shevkoplyas, L. Turner, M. Mayer, H. C. Berg and G. M. Whitesides, *Lab Chip*, 2008, **8**, 1888.
107 E. H. A. de Hoog, W. K. Kegel, A. van Blaaderen and H. N. W. Lekkerkerker, *Phys. Rev. E: Stat., Nonlinear, Soft Matter Phys.*, 2001, **64**, 021407.
108 A. E. Bailey, W. C. K. Poon, R. J. Christianson, A. B. Schofield, U. Gasser, V. Prasad, S. Manley, P. N. Segre, L. Cipelletti, W. V. Meyer, M. P. Doherty, S. Sankaran, A. L. Jankovsky, W. L. Shiley, J. P. Bowen, J. C. Eggers, C. Kurta, T. Lorik, P. N. Pusey and D. A. Weitz, *Phys. Rev. Lett.*, 2007, **99**, 205701.
109 D. G. A. L. Aarts, *Soft Matter*, 2007, **3**, 19–23.
110 C. P. Royall, S. R. Williams, T. Ohtsuka and H. Tanaka, *Nat. Mater.*, 2008, **7**, 556–561.
111 L. Assoud, F. Ebert, P. Keim, R. Messina, G. Maret and H. Löwen, *Phys. Rev. Lett.*, 2009, **102**, 238301.
112 K. G. Kang, M. P. Lettinga, Z. Dogic and J. K. G. Dhont, *Phys. Rev. E: Stat., Nonlinear, Soft Matter Phys.*, 2006, **74**, 026307.
113 R. J. Asaro and W. A. Tiller, *Metall. Trans.*, 1972, **3**, 1789.
114 M. A. Grinfeld, *Sov. Phys. Dokl.*, 1986, **31**, 831.
115 Z. F. Huang and K. R. Elder, *Phys. Rev. Lett.*, 2008, **101**, 158701.
116 K. A. Wu and P. W. Voorhees, *Phys. Rev. B*, 2009, **80**, 125408.
117 S. G. Yiantsios and B. G. Higgins, *Phys. Fluids*, 2006, **18**, 082103.
118 A. Würger, *Phys. Rev. Lett.*, 2007, **98**, 138301.
119 J. K. G. Dhont, S. Wiegand, S. Duhr and D. Braun, *Langmuir*, 2007, **23**, 1674–1683.
120 F. M. Weinert and D. Braun, *Phys. Rev. Lett.*, 2008, **101**, 168301.
121 J. Dzubiella and H. Löwen, *J. Phys.: Condens. Matter*, 2002, **14**, 9383.
122 C. N. Likos, Z. T. Németh and H. Löwen, *J. Phys.: Condens. Matter*, 1994, **6**, 10965.